Use of nitrogen and oxygen isotopes of dissolved nitrate to trace field-scale induced denitrification efficiency throughout an in-situ groundwater remediation strategy.

Rosanna Margalef-Marti, Raúl Carrey, Marta Viladés, Irene Jubany, Ester Vilanova, Roser Grau, Albert Soler, Neus Otero

Science of the total Environment, 2019, Volume 686, Pages 709-718
DOI: https://doi.org/10.1016/j.scitotenv.2019.06.003

Received date: 7 March 2019
Revised date: 31 May 2019
Accepted date: 1 June 2019
Available online: 5 June 2019

Use of nitrogen and oxygen isotopes of dissolved nitrate to trace field-scale induced denitrification efficiency throughout an in-situ groundwater remediation strategy

Rosanna Margalef-Marti[1], Raúl Carrey[1], Marta Viladés[2], Irene Jubany[3], Ester Vilanova[4], Roser Grau[5], Albert Soler[1], Neus Otero[1,6]

[1] Grup MAiMA, SGR Mineralogia Aplicada, Geoquímica i Geomicrobiologia, Departament de Mineralogia, Petrologia i Geologia Aplicada, Facultat de Ciències de la Terra, Universitat de Barcelona (UB), Barcelona (Spain).

[2] Sustainability Department, Fundació CTM Centre Tecnològic, Spain.

[3] Sustainability Area, Eurecat, Centre Tecnològic de Catalunya, Spain.

[4] Amphos 21 Consulting SL, Spain.

[5] Catalana de Perforacions, Spain.

[6] Serra Húnter Fellow, Generalitat de Catalunya, Spain.

ABSTRACT

In the framework of the Life+ InSiTrate project, a pilot-plant was established to demonstrate the viability of inducing in-situ heterotrophic denitrification to remediate nitrate (NO_3^-)-polluted groundwater. Two injection wells supplied acetic acid by pulses to an alluvial aquifer for 22 months. The monitoring was performed by regular sampling at three piezometers and two wells located downstream. In the present work, the pilot-plant monitoring samples were used to test the usefulness of the isotopic tools to evaluate the efficiency of the treatment. The laboratory microcosm experiments determined an isotopic fractionation (ε) for $N\text{-}NO_3^-$ of -12.6 ‰ and for $O\text{-}NO_3^-$ of -13.3 ‰. These $\varepsilon^{15}N_{NO3/N2}$ and $\varepsilon^{18}O_{NO3/N2}$ values were modelled by using a Rayleigh distillation equation to estimate the percentage of the induced denitrification at the pilot-plant while avoiding

a possible interference from dilution due to non-polluted water inputs. In some of the field samples, the induced NO_3^- reduction was higher than 50 % with respect to the background concentration. The field samples showed a reduced slope between $\delta^{18}O$-NO_3^- and $\delta^{15}N$-NO_3^- (0.7) compared to the laboratory experiments (1.1). This finding was attributed to the reoxidation of NO_2^- to NO_3^- during the treatment. The NO_3^- isotopic characterization also permitted the recognition of a mixture between the denitrified and partially or non-denitrified groundwater in one of the sampling points. Therefore, the isotopic tools demonstrated usefulness in assessing the implementation of the field-scale induced denitrification strategy.

Keywords: denitrification, electron donor, groundwater, isotopic fractionation, pilot-plant, remediation

1. Introduction

The scope of the anthropogenic disturbance of the nitrogen (N) cycle is conspicuous. Nitrate (NO_3^-) pollution is a current concern, as it has been related to ecological and human health disorders (Vitousek et al., 1997; Ward et al., 2005), and its presence in the groundwater is still increasingly large in many countries. The main sources of groundwater NO_3^- are linked to intensive use of synthetic and organic fertilizers and septic system leakage (Vitòria et al., 2008; Wassenaar, 1995). Some of the European directives that have arisen to mitigate the NO_3^- pollution (e.g., (2000/60/EC; 2006/118/EC; 91/676/EEC)) have focused on reducing the N inputs into the soil. However, due to the long residence time of N in the soil organic matter pool, the outcome of the agricultural management practices influencing the NO_3^- loading to the hydrosphere may be delayed for more than three decades (Sebilo et al., 2013). Therefore, water treatment is required to avoid the NO_3^- contamination impacts.

Denitrification has been shown to occur intrinsically throughout many environments, including aquifers, due to the ubiquity of the denitrifying microorganisms (Kraft et al.,

2011; Philippot et al., 2007; Richardson and Watmough, 1999). While oxidizing an electron donor, these microorganisms are able to reduce NO_3^- (electron acceptor) to gaseous N_2 through a series of enzyme-mediated reactions: $NO_3^- \rightarrow NO_2^- \rightarrow NO \rightarrow N_2O \rightarrow N_2$ (Knowles, 1982). The mandatory conditions, such as electron acceptor availability and low oxygen concentration, are commonly encountered in the contaminated aquifers, but the electron donor presence is usually a limiting factor (Rivett et al., 2008). Hence, one of the feasible treatments for NO_3^- removal involves inducing in-situ heterotrophic denitrification by supplying an organic carbon (C) source as an external electron donor. The specific organic C compound employed and its supply strategy plays a critical role in the resulting execution efficiency. Among other parameters, this compound influences the NO_3^- reduction rates and the by-product accumulation (Hallin and Pell, 1998; Wilderer et al., 1987), which is undesirable, given that intermediates, such as nitrite (NO_2^-) or nitrous oxide (N_2O), could be even more harmful than NO_3^- itself (Badr and Probert, 1993; De Beer et al., 1997; Rivett et al., 2008). Therefore, the remediation approach must avoid pollution swapping to ensure the safety of the treatment. Several strategies to induce the heterotrophic denitrification have already been implemented at the field-scale (e.g., by ethanol or formate injection (Borden et al., 2012; Smith et al., 2001)). Over the treatment period, it is crucial to control the induced NO_3^- reduction efficiency.

Chemical and isotopic characterization has been applied to calculate the efficiency of the field-scale bioremediation strategies (Vidal-Gavilan et al., 2013), as well as to trace the natural NO_3^- transformation processes (Aravena and Robertson, 1998; Otero et al., 2009). In the course of denitrification, the unreacted residual NO_3^- becomes enriched in the heavy isotopes ^{15}N and ^{18}O (Aravena and Robertson, 1998; Böttcher et al., 1990; Mariotti et al., 1981), distinguishing the biological attenuation from other processes, such as dilution due to non-polluted water inputs (e.g., from rainfall), that could also lead to a concentration decrease without influencing the isotopic signature. The isotopic fractionation of N and O from dissolved NO_3^- ($\varepsilon^{15}N_{NO3/N2}$ and $\varepsilon^{18}O_{NO3/N2}$) determined at

laboratory-scale, in denitrification experiments performed under controlled conditions, can be later applied at field-scale to estimate the NO_3^- attenuation significance during the intrinsic or induced denitrification (Böttcher et al., 1990; Mariotti et al., 1988). The isotopic characterization can also be used to determine the existence of undesired concurring processes, such as sulfate (SO_4^{2-}) reduction. Similarly to the case of NO_3^-, the isotopic composition of S and O from dissolved SO_4^{2-} allows to identify the occurrence of bacterial SO_4^{2-} reduction (BSR) by oxidation of an organic C electron donor, that could occur simultaneously to denitrification (Laverman et al., 2012; Strebel et al., 1990).

During the last decade, more than 50 % of the wells monitored by the Catalan Water Agency in the Maresme area (north-east Spain) presented NO_3^- concentrations above 50 mg/L (ACA, 2018), the threshold value set by the directive 98/83/EC. Despite the Maresme was designated a nitrogen vulnerable zone in 1998 and good agricultural practices were implemented, NO_3^- is still exceeding 200 mg/L in a number of wells (DECRET 136/2009; DECRET 283/1998). In the framework of the Life+ InSiTrate project, a pilot-plant was set up in Sant Andreu de Llavaneres (Maresme) to produce safe drinking water from NO_3^--polluted groundwater by inducing in-situ denitrification. The present study aims to test the usefulness of the isotopic tools to determine the denitrification efficiency during a long-term induced attenuation strategy at the pilot-plant. An intrinsic prior goal is to determine the $\varepsilon^{15}N_{NO3/N2}$ and $\varepsilon^{18}O_{NO3/N2}$ values at laboratory-scale by using the selected electron donor, as well as the sediment and groundwater from the polluted alluvial aquifer. Afterwards, the suitability of using ε values calculated from the laboratory-scale assays to evaluate the field-scale denitrification treatment efficiency will be discussed.

2. Pilot-plant description

The project site is located 10 m nearby the San Andreu de Llavaneres Creek. The pilot plant is placed in an alluvial aquifer, formed by Quaternary (Holocene) coarse sand and

104 silt sediments overlying an altered Paleozoic granite formation located at 40 m depth
105 (IGC, 2011). Before the biostimulation, the area was characterized by means of pumping
106 and tracing assays. The obtained permeability was between 70 and 100 m/d,
107 transmissivity was between 800 and 1000 m^2/d and the average porosity was 0.5. The
108 average aquifer temperature was 20.3 ºC (SD = 1.4). Prior to the treatment, the aquifer
109 showed aerobic conditions and natural NO_3^- attenuation was not observed, discarding
110 the availability of electron donors in the aquifer that could promote denitrification
111 intrinsically. The pilot-plant consisted of two electron donor injection wells (I1 and I2),
112 one treated water extraction well (EW) at an approximate distance of 30 m from the two
113 injection wells, three monitoring piezometers (PZ1, PZ2 and PZ3) between the injection
114 and the extraction wells, and one monitoring well (MW) downstream, located out of the
115 area affected by the biostimulation (**Figure 1**).

116 The in-situ heterotrophic denitrification stimulation was performed by adding acetic acid
117 (CH_3COOH) as an external electron donor. A variety of organic C compounds have been
118 tested at the laboratory-scale to identify suitable electron donor sources (Carrey et al.,
119 2018; Grau-Martínez et al., 2017; Peng et al., 2007). The CH_3COOH was selected by
120 considering the technical (previous column experiments), environmental (life cycle
121 assessment) and economic criteria (cost assessment) in the InSiTrate project. The
122 addition of this compound through the injection wells was performed by pulses to avoid
123 a high biomass accumulation that could lead to clogging issues, rather than a continuous
124 supply (Khan and Spalding, 2004). The total biostimulation period was 22 months.

125 **3. Methods**

126 *3.1. Laboratory experiments*

127 The laboratory batch experiments simulated the aquifer conditions by using sediment
128 and groundwater from the pilot-plant site. The groundwater was obtained from the MW

and stored at 4 ºC, whereas the sediment was obtained from the piezometer cores and stored frozen until use.

A total of 13 microcosms were settled by using 250 mL sealed glass flasks. The biostimulated microcosms (B1 to B10) were performed by adding CH_3COOH to the groundwater and sediment. Three types of control experiments were also performed. An untreated control (C1), to discard the intrinsic denitrification activity of the aquifer, contained groundwater and sediment from the study site with no CH_3COOH addition. Control C2, designed to discard the NO_3^- lixiviation from the sediment, contained MilliQ water and sediment with no CH_3COOH addition. Control C3 contained groundwater and CH_3COOH with no sediment, and was used to assess by comparison the contribution of the sediment on denitrification with respect to the groundwater. To attain the microbial stimulation, the CH_3COOH was injected at a 6.3 C/N ratio (w/w) according to previous laboratory experiments (data not shown) and results reported by other authors (Elefsiniotis and Li, 2006; Her and Huang, 1995). Also because this amount is representative of the CH_3COOH expected at the pilot-plant. However, the C/N ratio might not be totally homogeneous at field-scale due to dilution within the aquifer. Both at laboratory and field-scale, the total C employed for the overall NO_3^- removal process might be higher than expected from the stoichiometric C/N ratio (e.g., **Equation 1** proposed by Elefsiniotis and Li, 2006), as the CH_3COOH is also required for the water deoxygenation by heterotrophic bacteria before using NO_3^- as the electron acceptor. A detailed composition of the microcosms is shown in **Table 1**.

$$\frac{33}{140}NO_3^- + \frac{1}{4}CH_3COO^- + \frac{23}{140}H_2CO_3 \rightarrow \frac{1}{28}C_5H_7O_2N + \frac{1}{10}N_2 + \frac{6}{35}H_2O + \frac{34}{70}HCO_3^-$$

Equation 1

The head-space was purged with Ar after filling and sealing the flasks with GL45 caps holding silicone rubber PTFE-protected septa. All of the microcosms were maintained at 20 ºC in the darkness and with constant vibratory shaking throughout the experiment.

155 The biostimulated microcosms were sacrificed by turns at time intervals depending on
156 the denitrification dynamics until a complete NO_3^- and NO_2^- removal was achieved. The
157 samples from C3 were regularly obtained using a 1 mL syringe with a 25 G needle (BD).
158 The control microcosms were sacrificed at the end of the experiment.

159 *3.2. Field survey*

160 A total of forty-four samples were collected from five points in the pilot-plant (EW, PZ1,
161 PZ2, PZ3 and MW) in ten sampling campaigns, 9 performed during the twenty-two
162 months of the pilot-plant operation, and one performed two months after the end of
163 injections. The sampling intervals were established according to the pilot-plant operation
164 dynamics. In two of the sampling campaigns, two different depths (top and bottom) were
165 sampled for PZ1 and PZ2 to check differences in the treatment along the water column.
166 The monitoring wells and piezometers were purged prior to the sample collection by
167 removing three well volumes.

168 *3.3. Analyses*

169 Both the field survey and laboratory assays samples were filtered (0.2 µm Millipore®)
170 immediately when obtained and stored at 4 ºC until analysis, except for aliquots for the
171 isotopic characterization of N and O from NO_3^- that were preserved frozen at -20 ºC.

172 The determined chemical parameters were major anions (NO_2^-, NO_3^- and SO_4^{2-}),
173 analyzed by high-performance liquid chromatography (HPLC) (WATERS 515 pump and
174 WATERS IC-PAK ANIONS column with WATERS 432 and UV/V KONTRON detectors)
175 and ammonium (NH_4^+), analyzed by spectrophotometry (CARY 1E UV-visible) using the
176 indophenol blue method (Bolleter et al., 1961).

177 The analyzed isotopes were N and O of the dissolved NO_3^- ($\delta^{15}N\text{-}NO_3^-$ and $\delta^{18}O\text{-}NO_3^-$),
178 and S and O of the dissolved SO_4^{2-} ($\delta^{34}S\text{-}SO_4^{2-}$ and $\delta^{18}O\text{-}SO_4^{2-}$). The stable isotopes are
179 expressed using delta notation ($\delta = ((R_{sample}-R_{standard})/R_{standard})$, where R is the ratio

between the heavy and the light isotopes). The considered international standards were: Atmospheric N_2 (AIR) for $\delta^{15}N$, Vienna Standard Mean Oceanic Water (V-SMOW) for $\delta^{18}O$ and Vienna Canyon Diablo Troillite (V-CDT) for $\delta^{34}S$. The $\delta^{15}N\text{-}NO_3^-$ and $\delta^{18}O\text{-}NO_3^-$ composition was determined following the cadmium reduction method (McIlvin and Altabet, 2005; Ryabenko et al., 2009). Next, the N_2O was analyzed by using a Pre-Con (Thermo Scientific) coupled to a Finnigan MAT 253 Isotope Ratio Mass Spectrometer (IRMS, Thermo Scientific). For the SO_4^{2-} isotopic analysis, the dissolved SO_4^{2-} was precipitated as $BaSO_4$ (Dogramaci et al., 2001). The $\delta^{34}S\text{-}SO_4^{2-}$ was analyzed with a Carlo Erba Elemental Analyzer (EA) coupled in a continuous flow to a Finnigan Delta XP Plus IRMS, whereas the $\delta^{18}O\text{-}SO_4^{2-}$ was analyzed with a ThermoQuest high-temperature conversion analyzer (TC/EA) coupled in a continuous flow with a Finnigan Matt Delta XP Plus IRMS. According to Coplen (2011), several international and laboratory (CCiT) standards were interspersed among samples for the normalization of the isotopic results. For the $\delta^{15}N\text{-}NO_3^-$ and $\delta^{18}O\text{-}NO_3^-$ analysis the employed standards were USGS-32, USGS-34, USGS-35 and CCiT-IWS ($\delta^{15}N$ = +16.9 ‰, $\delta^{18}O$ = +28.5 ‰); for the $\delta^{34}S\text{-}SO_4^{2-}$ analyses, NBS-127, IAEA-SO-5, IAEA-SO-6, and CCiT-YCEM ($\delta^{34}S$ = +12.8 ‰); and for the $\delta^{18}O\text{-}SO_4^{2-}$ analysis, NBS-127, CCiT-YCEM ($\delta^{18}O$ = +17.6 ‰) and CCIT-ACID ($\delta^{18}O$ = +13.2 ‰). The reproducibility (1σ) of the samples, calculated from the standards systematically interspersed in the analytical batches, was ±1.0 ‰ for $\delta^{15}N\text{-}NO_3^-$, ±1.5 ‰ for $\delta^{18}O\text{-}NO_3^-$, ±0.2 ‰ for $\delta^{34}S\text{-}SO_4^{2-}$ and ±0.5 ‰ for $\delta^{18}O\text{-}SO_4^{2-}$.

The chemical and isotopic analyses were prepared in the MAiMA-UB research group laboratory and performed at the Centres Científics i Tecnològics of the Universitat de Barcelona (CCiT-UB).

3.4. Isotope data calculations

In the batch experiments, the isotopic fractionation was calculated by means of the Rayleigh distillation **Equation 2**. Thus, the $\varepsilon^{15}N_{NO3/N2}$ and $\varepsilon^{18}O_{NO3/N2}$ were obtained from

the slope of the linear correlation between the natural logarithm of the substrate remaining fraction ($Ln(C_{residual}/C_{initial})$, where C refers to the analyte concentration) and the determined isotope ratios ($Ln(R_{residual}/R_{initial})$, where $R = \delta+1$).

$$Ln\left(\frac{R_{residual}}{R_{initial}}\right) = \varepsilon \times Ln\left(\frac{C_{residual}}{C_{initial}}\right) \quad \textbf{Equation 2}$$

The percentage of NO_3^- attenuation caused by denitrification at field-scale was estimated by using these $\varepsilon^{15}N_{NO3/N2}$ and $\varepsilon^{18}O_{NO3/N2}$ calculated under closed system conditions and **Equation 3**, which is derived from the Rayleigh fractionation model (**Equation 2**). The quantification of pollutants degradation by using Rayleigh derived equations has been applied elsewhere (Meckenstock et al., 2004; Otero et al., 2009; Schmidt et al., 2004; Vidal-Gavilan et al., 2013).

$$DEN\ \% = \left[1 - \left(\frac{C_{residual}}{C_{initial}}\right)\right] \times 100 = \left[1 - \left(\frac{R_{residual}}{R_{initial}}\right)^{\left(\frac{1}{\varepsilon}\right)}\right] \times 100 \quad \textbf{Equation 3}$$

4. Results and discussion

4.1. Laboratory-scale experiments

4.1.1. NO_3^- reduction by CH_3COOH

The NO_3^- and NO_2^- lixiviation from the sediment was discarded, since the concentration of both compounds was below the detection limit in the C2 microcosm (Milli-Q water + sediment) after 102 hours of incubation. The C1 microcosm (groundwater + sediment) showed no depletion of the initial NO_3^- concentration, thereby ruling out intrinsic denitrification activity from the aquifer groundwater or sediment in the microcosms due to the presence of trace electron donors. Thus, the observed NO_3^- reduction in the biostimulated microcosms (B1-B10) was considered to be caused by the CH_3COOH injection (**Figure 2**). All data obtained from the laboratory-scale experiments is presented in the Supporting Information **Table S1**.

229 The bacterial NO_3^- reduction in the biostimulated experiments (B1-B10) was initiated
230 between 32 and 47 hours after the electron donor injection. The initial lag period was the
231 acclimation time for the establishment of a heterotrophic bacterial community after
232 unfreezing the sediment and merging it with the groundwater. Also, all of the oxygen
233 present in the groundwater had to be consumed before using NO_3^- as the electron
234 acceptor. The concentration analysis showed that after the onset, NO_3^- reduction
235 proceeded rapidly until NO_3^- was completely consumed 70 hours after biostimulation,
236 yielding an average NO_3^- removal rate of 0.30 mmol/(dm^3·day) (calculated for the total
237 length of the experiment including the acclimation period). As the NO_3^- concentration
238 started to decrease, NO_2^- progressively accumulated, reaching a 0.26 mM maximum
239 peak, which is 30 % of the initial N-NO_3^- concentration, approximately 50 hours after the
240 injection. The transient NO_2^- accumulation has been widely reported to occur during the
241 laboratory (Calderer et al., 2010; Carrey et al., 2013; Her and Huang, 1995) and field-
242 scale (Critchley et al., 2014; Gierczak et al., 2007; Vidal-Gavilan et al., 2013)
243 denitrification studies. The NO_2^- usually accumulates until the bacterial communities
244 adapt to the new redox conditions caused by the electron donor addition. One of the
245 reasons is an earlier induction of the NO_3^- reductases with respect to the NO_2^- reductases
246 (Zumft, 1997 and references therein). After 50 hours, the NO_2^- progressively decreased
247 and was completely consumed when the NO_3^- removal was also accomplished. The NO_3^-
248 reduction and NO_2^- accumulation observed can also be produced by dissimilatory NO_3^-
249 reduction to NH_4^+ (DNRA). However, the NH_4^+ detected in the microcosms was low (up
250 to 0.04 mM). Therefore, DNRA did not contribute significantly to the NO_3^- concentration
251 decrease in the microcosms, pointing out denitrification as the main reaction.

252 In the biostimulated microcosm lacking sediment (C3), a complete NO_3^- reduction was
253 also achieved, but the NO_2^- accumulation increased significantly. A 0.76 mM NO_2^- peak,
254 which is 86 % of the initial N-NO_3^-, was reached after 84 hours and decreased rapidly
255 until depletion was complete (**Figure 2**). After 95 hours, the NO_3^- and NO_2^- levels were

below the detection limit. The average NO_3^- removal rate was 0.22 mmol/(dm^3·day), which is lower than the obtained from the biostimulated microcosms containing sediment. Although the groundwater alone provided the needed conditions to achieve a complete denitrification in the CH_3COOH amended microcosms, the sediment increased significantly the attenuation efficiency. The lowered NO_3^- removal rate and the increased magnitude of the NO_2^- peak in the microcosms lacking sediment might be attributed to a diminished initial bacterial content that might result in lower and/or different bacterial species growth stimulation. Other reasons could include a buffering effect promoted by the sediment or the influence of the sediment surface upon reactivity.

4.1.2. Isotopic fractionation calculation

While being progressively reduced, the isotopic composition of the residual NO_3^- in the biostimulated microcosms became higher in both ^{15}N and ^{18}O. The initial groundwater values for $\delta^{15}N\text{-}NO_3^-$ and $\delta^{18}O\text{-}NO_3^-$ of +5.1 ‰ and +3.6 ‰, respectively, increased over the experimental period to +29.9 ‰ and +30.8 ‰, respectively. The calculated ε values, were -12.6 ‰ (r^2 = 0.99) for $\varepsilon^{15}N_{NO3/N2}$ and -13.3 ‰ (r^2 = 0.96) for $\varepsilon^{18}O_{NO3/N2}$, resulting in a $\varepsilon^{15}N/\varepsilon^{18}O$ of 0.95 (**Figure 3**). These values fall within the reported range for the heterotrophic denitrification (from -5.4 ‰ to -26.6 ‰ for $\varepsilon^{15}N_{NO3/N2}$, from -4.8 ‰ to -23.7 ‰ for $\varepsilon^{18}O_{NO3/N2}$, and from 0.6 to 1.0 for $\varepsilon^{15}N/\varepsilon^{18}O$ (Granger et al., 2008; Wunderlich et al., 2012)).

Carrey et al., (2013); Torrentó et al., (2011) and Vidal-Gavilan et al., (2013) applied the $\varepsilon^{15}N_{NO3/N2}$ and $\varepsilon^{18}O_{NO3/N2}$ values obtained from laboratory batch experiments, using either intrinsic or added electron donors, to quantify the extent of natural or induced groundwater denitrification. By using the laboratory derived ε values to estimate the induced NO_3^- reduction, interferences from processes other than denitrification that could also lead to a concentration decrease (e.g., dilution due to water discharges from rainfall) are avoided. For the pilot-plant study, we considered it appropriate to apply the $\varepsilon^{15}N_{NO3/N2}$

and $\varepsilon^{18}O_{NO3/N2}$ calculated from the laboratory experiments because groundwater and sediment from the aquifer were used and consequently, a similar electron acceptor availability and stimulated bacterial community with respect to the field was expected.

4.2. Field survey

4.2.1. Isotopic dynamic in the pilot-plant

The sampling campaigns began one month after the CH_3COOH injections started and continued for two years, with the last survey being performed two months after stopping the injections. All data obtained from the pilot-plant are presented in the Supporting Information **Table S2**. The unaffected MW (n = 6) presented average values of 0.9 mM (SD = 0.04) for NO_3^- concentration, +6.3 ‰ (SD = 1.3) for $\delta^{15}N\text{-}NO_3^-$ and +4.2 ‰ (SD = 0.9) for $\delta^{18}O\text{-}NO_3^-$, which were considered to be the groundwater NO_3^- background composition. The isotopic values of the MW fall in the soil NO_3^- area (**Figure 4**) reported by Vitòria et al. (2004) and references therein. However, the high NO_3^- concentration suggested an anthropogenic origin. In a previous study located in a nearby area with intensive application of chemical fertilizers, Vitòria et al. (2005) demonstrated that the combined occurrence of volatilization and nitrification resulted in groundwater NO_3^- with $\delta^{15}N\text{-}NO_3^-$ and $\delta^{18}O\text{-}NO_3^-$ in the range of soil NO_3^-. Therefore, the isotopic values of the MW suggested that the NO_3^- pollution in the studied aquifer was derived from N inorganic fertilizer that had been volatilized and nitrified (**Figure 4**).

Following the electron donor addition, the three monitoring piezometers showed a marked NO_3^- decrease. PZ1 and PZ2 reached NO_3^- concentrations below 0.3 mM from the 10th operation month and until the last injection. PZ3 also showed a decreasing trend but with a NO_3^- concentration higher than PZ1 and PZ2 and a temporal trend showing fluctuations (**Figure 5**). Contrarily, a flat trend in the NO_3^- evolution was observed at the EW (**Figure 5**), showing concentrations between 13 % and 33 % lower than the MW. In the two-depth sampling at PZ1 in the 17th month, no significant NO_3^- concentration

differences were observed between the bottom and the top samples, and in both cases, NO_3^- was almost completely denitrified. However, at PZ2 in the 19th month, the bottom sample showed a doubled NO_3^- concentration compared to the top sample. In all the samples NO_2^- was below 0.02 mM (Supporting Information **Figure S1**) and NH_4^+ was below 0.01 mM. Therefore, pollution swapping due to accumulation of these compounds was discarded in the pilot-plant.

In response to the NO_3^- attenuation in the piezometers, the $\delta^{15}N\text{-}NO_3^-$ and $\delta^{18}O\text{-}NO_3^-$ increased. The temporal dynamics of the NO_3^- isotopic composition in the pilot-plant is shown in the Supporting Information **Figure S2**. The highest values were measured at PZ1, showing a $\delta^{15}N\text{-}NO_3^-$ and $\delta^{18}O\text{-}NO_3^-$ of +22.1 ‰ and +14.7 ‰, respectively (**Figure 4**). Note that four samples were below the limit of concentration necessary for the isotopic analysis (0.05 mM), and could have even shown higher isotopic values. The $\delta^{15}N\text{-}NO_3^-$ and $\delta^{18}O\text{-}NO_3^-$ in the EW samples were close to the MW average values (**Figure 4**). Two months after the end of the treatment, the EW and PZ3 recovered to NO_3^- background concentrations and isotopic values, but PZ1 and PZ2 still showed evidence of denitrification (**Figure 5**).

When NO_3^- is completely removed from the environment, the excess organic C can trigger BSR, provoking a decrease in the treated water quality due to the production of H_2S. However, the coexistence of denitrification and BSR in the presence of an electron donor has also been demonstrated. Laverman et al., (2012) observed that the ratio between the BSR rate and the denitrification rate tends to increase at high organic matter concentrations. As in the studied pilot-plant, organic matter was available, BSR could occur simultaneously to denitrification. The isotopic results from a subset of the pilot-plant samples showed a 0.4 (r^2 = 0.93) slope from the regression line between $\delta^{18}O\text{-}SO_4^{2-}$ and $\delta^{34}S\text{-}SO_4^{2-}$ (**Figure 6**), which is in the range of the slopes from 0.25 to 0.7 reported in the literature for BSR (Aharon and Fu, 2000). However, the samples with the lowest SO_4^{2-} concentration (~ 1 mM) were not the most enriched in $\delta^{18}O\text{-}SO_4^{2-}$ and $\delta^{34}S$-

335 SO_4^{2-} and vice versa (maximum measured SO_4^{2-} was ~ 5 mM). Since there was surplus
336 NO_3^- in the groundwater and due to the lack of correlation between the SO_4^{2-} chemical
337 and isotopic data, BSR did not likely play a significant role at the pilot-plant. In the same
338 context of water quality, the presence of remaining CH_3COOH at a harmful level for
339 consumption was also discarded due to the excess of electron acceptors such as NO_3^-
340 or SO_4^{2-} in groundwater since denitrification was never completed at the EW.

341 *4.2.2. Isotopic fractionation from the laboratory to field-scale*

342 A subset of the campaigns considered to be representative of the treatment efficiency
343 evaluation are discussed. As previously stated, the average NO_3^- concentration, δ^{15}N-
344 NO_3^- and δ^{18}O-NO_3^- of the MW were used as the initial composition, since the MW was
345 considered to be unaffected by the treatment. During the initial operation (1st month), the
346 NO_3^- isotopic composition did not show a relevant δ^{15}N or δ^{18}O enrichment, indicating
347 that the denitrification was not significant (**Figure 7A**). After seven operation months,
348 and until the end of the monitoring period, a clear δ^{15}N-NO_3^- and δ^{18}O-NO_3^- enrichment
349 evidenced the biological NO_3^- reduction at the pilot-plant. The degree of reduction
350 depended on the specific point and sampling campaign. According to the concentration
351 measured, more than 95 % NO_3^- was reduced at PZ1 in the 14th, 17th and 19th months,
352 and at PZ2 in the 17th month. However, those samples could not be isotopically analyzed,
353 since the NO_3^- concentration was below the detection limit (0.05 mM). The isotopic
354 composition of the remnant samples determined that the denitrification at the pilot-plant
355 piezometers reached a significance of approximately 50 % (e.g., 19th month (**Figure**
356 **7D**)). Even two months after stopping the biostimulation (month 24th), more than a 50 %
357 of the groundwater NO_3^- was still denitrified at PZ1 (**Figure 7E**).

358 For each of the pilot-plant samples, the denitrification % calculated by using the isotopic
359 data was compared to the % calculated by using the NO_3^- concentration (Supporting
360 Information **Table S2**). For most of the pilot-plant samples (e.g., 2nd, 11th, 12th and 24th

361 month campaigns), the calculated % from the chemical data was higher than the %
362 obtained from the isotopic data, as expected from the influence of dilution due to non-
363 polluted water inputs from rainfall (Supporting information **Figure S3**). Four of the
364 samples showed highly similar % values (<5 % difference), suggesting that in these
365 cases dilution did not occur. Contrarily, in five samples, the % calculated from the NO_3^-
366 concentration was lower compared to the % from the isotopic data. This variation might
367 be produced by different reasons, depending on the characteristics of the samples
368 involved. For PZ1 and PZ3 from the 1st month campaign, the denitrification had not still
369 begun, and the lower % could be derived from the intrinsic aquifer variability due to the
370 use of an average value for the MW to draw the DEN % line instead of the specific MW
371 value for each of the sampling campaigns. For PZ1 and PZ3 from the 7th month campaign
372 and PZ3 from the 19th month campaign, the reason could be a mixing effect between
373 treated and non-treated groundwater.

374 Chemical and isotopic data of the EW evidenced a mixing between treated and non-
375 treated groundwater. In the 7th month campaign, a slight isotopic enrichment and NO_3^-
376 concentration decrease was observed at the EW with respect to the MW, being indicative
377 of the denitrification occurrence (**Figure 7B**). However, from the 7th month onward,
378 despite the lower NO_3^- concentration at the EW with respect to the MW, the isotopic data
379 did not show significant differences (e.g., 12th or 19th month) (**Figure 7C and 7D**). The
380 reason is that the groundwater extracted at the EW was a mix of denitrified groundwater
381 from PZ1 and PZ2 located upstream and untreated water from the MW located
382 downstream, due to a depression cone at EW forced by the water extraction (**Figure 1**).
383 To determine the contribution to EW, a theoretical mixing between 30 % of PZ2 and 70
384 % of MW was estimated using chemical and isotopic data, and was compared with the
385 measured values (**Table 2**). Measured results are fairly in agreement with the estimated
386 ones throughout the monitoring period. This mixing between treated and non-treated
387 groundwater was also observed along the water column. During the two-depth sampling

388 at PZ2 (19th month), no significant isotopic composition differences were observed,
389 although the measured NO_3^- concentrations were 0.2 and 0.1 mM in the bottom and top
390 samples, respectively (**Figure 7D**). In these two samples, the denitrification % obtained
391 with the isotopic data (~50 %) might also result from mixing between the partially and
392 non-denitrified groundwater. Therefore, the attenuation in the water column might be
393 heterogeneous with reactive microsites where NO_3^- can be completely removed. In the
394 same campaign (19th month), PZ3 showed a similar isotopic composition to the two
395 samples from PZ2, but presented a remarkably higher NO_3^- concentration, reinforcing
396 the idea of the groundwater mixing between the partially and non-denitrified
397 groundwater. In PZ3, the denitrified water had a lesser contribution compared to PZ2.
398 Due to the effect produced by this mixing, the obtained field-scale denitrification % from
399 the laboratory determined $\varepsilon^{15}N_{NO3/N2}$ and $\varepsilon^{18}O_{NO3/N2}$ must be considered an estimation,
400 and not a precise calculation.

401 *4.2.3. NO_2^- reoxidation evidence from the isotopic results*

402 The determined slope between $\delta^{18}O\text{-}NO_3^-$ and $\delta^{15}N\text{-}NO_3^-$ from the field samples (0.7 (r^2
403 = 0.95)) and the slope from the batch experiments (1.1 (r^2 = 0.99)) agree with the already
404 reported slopes of nearly 0.5 for groundwater denitrification studies at field-scale (Chen
405 and MacQuarrie, 2005; Critchley et al., 2014; Otero et al., 2009), and nearly 1.0 for
406 laboratory studies (Carrey et al., 2013; Grau-Martínez et al., 2017; Wunderlich et al.,
407 2012). However, the slopes around 0.5 have also been found in pure culture laboratory
408 experiments. The lower $\varepsilon^{18}O_{NO3/N2}$ compared to $\varepsilon^{15}N_{NO3/N2}$ can be caused by the use of
409 the periplasmic NO_3^- reductase (NAP) instead of the membrane bound NO_3^- reductase
410 (NAR) (Granger et al., 2008), or by the oxidation of the intermediates NO_2^- and NH_4^+ to
411 NO_3^- (Granger and Wankel, 2016; Wunderlich et al., 2013). It is widely assumed that
412 NAP has an insignificant role in the aquifer environments where anaerobic conditions
413 are prevalent, and because it does not involve a metabolic energy generation process
414 (Moreno-Vivián et al., 1999). The denitrification and the DNRA coupled to the anaerobic

ammonium oxidation (anammox) can occur concomitantly in freshwater environments (Castro-Barros et al., 2017; Jones et al., 2017). However, the DNRA in the pilot-plant was rather unimportant since NO_3^- did not achieve complete reduction. The DNRA is favored at high C/N ratios, when NO_3^- is limited instead of the electron donor (Giles et al., 2012; Jones et al., 2017; Kelso et al., 1997). Therefore, the lower slope observed at the field-scale is likely related to the NO_2^- reoxidation which is consistent with the possibility of oxygen diffusion in groundwater compared to the laboratory microcosms.

The $\delta^{18}O$ of some dissolved oxygenated compounds, such as NO_2^-, can be equilibrated with the $\delta^{18}O$-H_2O (Granger and Wankel, 2016; Kool et al., 2007). If the intermediate NO_2^- reoxidates to NO_3^-, the resulting $\delta^{18}O$-NO_3^- will be dependent on the $\delta^{18}O$ of the NO_3^- source, the $\delta^{18}O$ of the groundwater, the kinetic isotopic effects produced during the denitrification and during the water atom incorporation by the oxidoreductase throughout the NO_2^- oxidation. Considering a $\delta^{18}O$-H_2O ranging from -7 to -4 ‰ in the studied area and the $\delta^{18}O$-NO_3^- average composition of the samples obtained from the unaffected MW being +4.2 ‰ (SD = 0.9), a decreased $\varepsilon^{18}O_{NO3/N2}$ is expected in the pilot-plant if the intermediate NO_2^- reoxidates to NO_3^-.

Several samples from the field site showed lower $\delta^{18}O$-NO_3^- values than expected, considering the denitrification slope calculated using the microcosm experiments (e.g., 7th, 12th and 19th month) (**Figure 7B, 7C and 7D**). This finding can be explained as the result of the NO_2^- reoxidation to NO_3^- throughout the remediation treatment. The low or null NO_2^- detection throughout the pilot-plant operation (Supporting Information, **Figure S2**) seemed consistent with the NO_2^- reoxidation, which is positive from a groundwater quality perspective. The shift in the slope throughout the induced denitrification treatment can provide information regarding the relevance of the NO_2^- reoxidation process at the field-scale. The $\delta^{15}N$-NO_3^- and $\delta^{18}O$-NO_3^- values close to the theoretical DEN % line might point to a direct NO_2^- reduction to gaseous N products, while lower $\delta^{18}O$-NO_3^- values might point to the NO_2^- reoxidation. By checking each of the sampling campaigns

separately, slopes near 0.5 were generally observed during the initial biostimulation (e.g., 7th month, 0.5 slope (r^2 = 0.8)) (**Figure 7B**), which became closer to 1.0 throughout the pilot-plant operation (e.g., 19th month, 0.8 slope (r^2 = 1.0)) (**Figure 7D**). At the last sampling campaign, corresponding to the recovery period after stopping the CH_3COOH injections, the slope was again closer to 0.5 (24th month, 0.6 slope (r^2 = 1.0)) (**Figure 7E**).

An unsolved question is the effect of the biotic and abiotic NO_2^- oxidation to NO_3^- upon $\delta^{15}N\text{-}NO_3^-$ throughout denitrification in groundwater. It is expected that the possible effect upon $\delta^{15}N\text{-}NO_3^-$ would be lower than the observed for $\delta^{18}O\text{-}NO_3^-$ during the abiotic NO_2^- oxidation, enabling the $\delta^{18}O\text{-}NO_3^-$ versus $\delta^{15}N\text{-}NO_3^-$ slope to decrease. For the biotic NO_2^- oxidation, an inverse isotopic fractionation for the $\delta^{15}N$ (and also for the $\delta^{18}O$) was observed during the NO_2^- oxidation to NO_3^- mediated by the marine species *Nitrococcus mobilis* (Buchwald and Casciotti, 2010; Casciotti, 2009). Consequently, when the NO_2^- reoxidation is observed during the in-situ groundwater remediation strategies, the denitrification significance might be biased if estimated by using the laboratory isotopic fractionation data.

5. Conclusions

After the implementation of an in-situ groundwater remediation strategy by CH_3COOH injections (InSiTrate project), the induced denitrifying activity reached NO_3^- concentrations below the threshold for water consumption. The $\varepsilon^{15}N_{NO3/N2}$ and $\varepsilon^{18}O_{NO3/N2}$ values obtained from the microcosm experiments allowed assessing the denitrification efficacy at the pilot-plant while avoiding the interference derived from dilution due to non-polluted water inputs. At the pilot-plant, more than a 50 % of the background NO_3^- was reduced due to the induced heterotrophic denitrification. The isotopic results allowed to detect a mixture between the denitrified and non-denitrified groundwater at the EW. However, a limitation of the application of the isotopes to evaluate the treatment efficacy

468 is that the denitrification significance could be underestimated due to the effect provoked
469 by the mixing of non-denitrified groundwater with partially denitrified groundwater. The
470 lower slope between $\delta^{18}O\text{-}NO_3^-$ and $\delta^{15}N\text{-}NO_3^-$ observed in the field (0.7) compared to
471 the laboratory (1.1) was attributed to the NO_2^- reoxidation to NO_3^-. However, the effect of
472 the NO_2^- reoxidation upon $\delta^{15}N\text{-}NO_3^-$ is still unclear, and it is unknown in which measure
473 the $\delta^{18}O\text{-}NO_3^-$ values resulting from the NO_2^- reoxidation can be firmly extrapolated to
474 the calculated DEN % line. In summary, the $\delta^{15}N\text{-}NO_3^-$ and $\delta^{18}O\text{-}NO_3^-$ analysis provides
475 a valuable tool to assess the induced denitrification strategies at the field-scale by means
476 of the laboratory calculated $\varepsilon^{15}N_{NO3/N2}$ and $\varepsilon^{18}O_{NO3/N2}$. However, attention must be focused
477 on the hydrogeological and biochemical effects that could influence the results and thus
478 the remediation strategies evaluation.

479 **ACKNOWLEDGMENTS**

480 This work has been financed by the following projects: REMEDIATION (CGL2014-
481 57215-C4) and PACE-ISOTEC (CGL2017-87216-C4-1-R), financed by the Spanish
482 Government and AEI/FEDER from the UE; MAG (2017-SGR-1733) from the Catalan
483 Government and LIFE Project InSiTrate (LIFE12 ENV/ES/000651). R. Margalef-Marti is
484 grateful to the Spanish Government for the Ph.D. grant BES-2015-072882. We would
485 like to thank the CCiT-UB for providing analytical support.

486 **REFERENCES**

487 2000/60/EC, 2000. Water Framework Directive [WWW Document]. Off. J. Eur. Comm.
488 URL http://ec.europa.eu/environment/index_en.htm (accessed 4.9.17).

489 2006/118/EC, 2006. Groundwater Directive. Council Directive 2006/118/EC, of 12
490 December 2006, on the protection of groundwater against pollution and
491 deterioration [WWW Document]. Off. J. Eur. Comm. URL
492 http://ec.europa.eu/environment/index_en.htm (accessed 4.9.17).

91/676/EEC, 1991. Nitrates Directive. Council Directive 91/676/EEC of 12 December 1991, concerning the protection of waters against pollution caused by nitrates from agricultural sources. [WWW Document]. Off. J. Eur. Comm. URL http://ec.europa.eu/environment/index_en.htm (accessed 4.9.17).

98/83/EC, 1998. Drinking Water Directive. Council Directive 98/83/EC, of 3 November 1998, on the quality of water intended for human consumption. [WWW Document]. Off. J. Eur. Comm. URL http://ec.europa.eu/environment/index_en.htm (accessed 4.9.17).

ACA, 2018. Consulta de dades de control de la qualitat i la quantitat de l'aigua al medi de l'Agència Catalana de l'Aigua (ACA). [WWW Document].

Aharon, P., Fu, B., 2000. Microbial sulfate reduction rates and sulfur and oxygen isotope fractionations at oil and gas seeps in deepwater Gulf of Mexico. Geochim. Cosmochim. Acta 64, 233–246. https://doi.org/10.1016/S0016-7037(99)00292-6

Aravena, R., Robertson, W.D., 1998. Use of multiple isotope tracers to evaluate denitrification in ground water: study of nitrate from a large-flux septic system plume. Ground Water 36, 975–982.

Badr, O., Probert, S.D., 1993. Environmental impacts of atmospheric nitrous oxide. Appl. Energy. https://doi.org/10.1016/0306-2619(93)90018-K

Bolleter, W.T., Bushman, C.J., Tidwell, P.W., 1961. Spectrophotometric Determination of Ammonia as Indophenol. Anal. Chem. 33, 592–594. https://doi.org/10.1021/ac60172a034

Borden, A.K., Brusseau, M.L., Carroll, K.C., McMillan, A., Akyol, N.H., Berkompas, J., Miao, Z., Jordan, F., Tick, G., Waugh, W.J., Glenn, E.P., 2012. Ethanol addition for enhancing denitrification at the uranium mill tailing site in Monument Valley, AZ. Water. Air. Soil Pollut. 223, 755–763. https://doi.org/10.1007/s11270-011-

518 0899-1

519 Böttcher, J., Strebel, O., Voerkelius, S., Schmidt, H.-L., 1990. Using isotope
520 fractionation of nitrate-nitrogen and nitrate-oxygen for evaluation of microbial
521 denitrification in a sandy aquifer. J. Hydrol. 114, 413–424.
522 https://doi.org/10.1016/0022-1694(90)90068-9

523 Buchwald, C., Casciotti, K.L., 2010. Oxygen isotopic fractionation and exchange during
524 bacterial nitrite oxidation. Limnol. Oceanogr. 55, 1064–1074.
525 https://doi.org/10.4319/lo.2010.55.3.1064

526 Calderer, M., Gibert, O., Martí, V., Rovira, M., De Pablo, J., Jordana, S., Duro, L.,
527 Guimerá, J., Bruno, J., 2010. Denitrification in presence of acetate and glucose for
528 bioremediation of nitrate-contaminated groundwater. Environ. Technol. 31, 799–
529 814. https://doi.org/10.1080/09593331003667741

530 Carrey, R., Otero, N., Soler, A., Gómez-Alday, J.J., Ayora, C., 2013. The role of Lower
531 Cretaceous sediments in groundwater nitrate attenuation in central Spain: Column
532 experiments. Appl. Geochemistry 32, 142–152.
533 https://doi.org/10.1016/j.apgeochem.2012.10.009

534 Carrey, R., Rodríguez-Escales, P., Soler, A., Otero, N., 2018. Tracing the role of
535 endogenous carbon in denitrification using wine industry by-product as an external
536 electron donor: Coupling isotopic tools with mathematical modeling. J. Environ.
537 Manage. 207, 105–115. https://doi.org/10.1016/j.jenvman.2017.10.063

538 Casciotti, K.L., 2009. Inverse kinetic isotope fractionation during bacterial nitrite
539 oxidation. Geochim. Cosmochim. Acta 73, 2061–2076.
540 https://doi.org/10.1016/j.gca.2008.12.022

541 Castro-Barros, C.M., Jia, M., van Loosdrecht, M.C.M., Volcke, E.I.P., Winkler, M.K.H.,
542 2017. Evaluating the potential for dissimilatory nitrate reduction by anammox

543 bacteria for municipal wastewater treatment. Bioresour. Technol. 233, 363–372.
544 https://doi.org/10.1016/j.biortech.2017.02.063

545 Chen, D.J.Z., MacQuarrie, K.T.B., 2005. Correlation of delta N-15 and delta O-18 in
546 NO_3^- during denitrification in groundwater. J. Environ. Eng. Sci. 4, 221–226.

547 Coplen, T.B., 2011. Guidelines and recommended terms for expression of stable-
548 isotope-ratio and gas-ratio measurement results. Rapid Commun. Mass
549 Spectrom. 25, 2538–2560. https://doi.org/10.1002/rcm.5129

550 Critchley, K., Rudolph, D.L., Devlin, J.F., Schillig, P.C., 2014. Stimulating in situ
551 denitrification in an aerobic, highly permeable municipal drinking water aquifer. J.
552 Contam. Hydrol. 171, 66–80. https://doi.org/10.1016/j.jconhyd.2014.10.008

553 De Beer, D., Schramm, A., Santegoeds, C.M., Kühl, M., 1997. A nitrite microsensor for
554 profiling environmental biofilms. Appl. Environ. Microbiol. 63, 973–977.

555 DECRET 136/2009, 2009. DECRET 136/2009, d'1 de setembre, d'aprovació del
556 programa d'actuació aplicable a les zones vulnerables en relació amb la
557 contaminació de nitrats que procedeixen de fonts agràries i de gestió de les
558 dejeccions ramaderes [WWW Document]. URL
559 https://portaljuridic.gencat.cat/ca/pjur_ocults/pjur_resultats_fitxa/?action=fitxa&doc
560 umentId=478701&language=ca_ES

561 DECRET 283/1998, 1998. DECRET 283/1998, de 21 d'octubre, de designació de les
562 zones vulnerables en relació amb la contaminació de nitrats procedents de fonts
563 agràries. [WWW Document]. URL
564 https://dogc.gencat.cat/ca/pdogc_canals_interns/pdogc_resultats_fitxa/?document
565 Id=179342&language=ca_ES&action=fitxa (accessed 2.5.19).

566 Dogramaci, S.., Herczeg, A.., Schiff, S.., Bone, Y., 2001. Controls on $\delta^{34}S$ and $\delta^{18}O$ of
567 dissolved sulfate in aquifers of the Murray Basin, Australia and their use as

indicators of flow processes. Appl. Geochemistry 16, 475–488. https://doi.org/10.1016/S0883-2927(00)00052-4

Elefsiniotis, P., Li, D., 2006. The effect of temperature and carbon source on denitrification using volatile fatty acids. Biochem. Eng. J. 28, 148–155. https://doi.org/10.1016/j.bej.2005.10.004

Gierczak, R., Devlin, J.F., Rudolph, D.L., 2007. Field test of a cross-injection scheme for stimulating in situ denitrification near a municipal water supply well. J. Contam. Hydrol. 89, 48–70. https://doi.org/10.1016/j.jconhyd.2006.08.001

Giles, M., Morley, N., Baggs, E.M., Daniell, T.J., 2012. Soil nitrate reducing processes - Drivers, mechanisms for spatial variation, and significance for nitrous oxide production. Front. Microbiol. 3, 1–16. https://doi.org/10.3389/fmicb.2012.00407

Granger, J., Sigman, D.M., Lehmann, M.F., Tortell, P.D., 2008. Nitrogen and oxygen isotope fractionation during dissimilatory nitrate reduction by denitrifying bacteria. Limnol. Oceanogr. 53, 2533–2545. https://doi.org/10.4319/lo.2008.53.6.2533

Granger, J., Wankel, S.D., 2016. Isotopic overprinting of nitrification on denitrification as a ubiquitous and unifying feature of environmental nitrogen cycling. Proc. Natl. Acad. Sci. 113, E6391–E6400. https://doi.org/10.1073/pnas.1601383113

Grau-Martínez, A., Torrentó, C., Carrey, R., Rodríguez-Escales, P., Domènech, C., Ghiglieri, G., Soler, A., Otero, N., 2017. Feasibility of two low-cost organic substrates for inducing denitrification in artificial recharge ponds: Batch and flow-through experiments. J. Contam. Hydrol. 198, 48–58. https://doi.org/10.1016/j.jconhyd.2017.01.001

Hallin, S., Pell, M., 1998. Metabolic properties of denitrifying bacteria adapting to methanol and ethanol in activated sludge. Water Res. 32, 13–18. https://doi.org/10.1016/S0043-1354(97)00199-1

Her, J.J., Huang, J.S., 1995. Influences of carbon source and C/N ratio on nitrate/nitrite denitrification and carbon breakthrough. Bioresour. Technol. 54, 45–51. https://doi.org/10.1016/0960-8524(95)00113-1

Jones, Z.L., Jasper, J.T., Sedlak, D.L., Sharp, J.O., 2017. Sulfide-Induced Dissimilatory Nitrate Reduction to Ammonium Supports Anaerobic Ammonium Oxidation (Anammox) in an Open-Water Unit Process Wetland 83, 1–14.

Kelso, B.H.L., Smith, R. V., Laughlin, R.J., Lennox, S.D., 1997. Dissimilatory nitrate reduction in anaerobic sediments leading to river nitrite accumulation. Appl. Environ. Microbiol. 63, 4679–4685.

Khan, I.A., Spalding, R.F., 2004. Enhanced in situ denitrification for a municipal well. Water Res. 38, 3382–3388. https://doi.org/10.1016/j.watres.2004.04.052

Knowles, R., 1982. Denitrification. Microbiol. Rev. 46, 43–70.

Kool, D.M., Wrage, N., Oenema, O., Dolfing, J., Van Groenigen, J.W., 2007. Oxygen exchange between (de)nitrification intermediates and H_2O and its implications for source determination of NO_3^- and N_2O: a review. Rapid Commun. Mass Spectrom. 21, 3569–3578. https://doi.org/10.1002/rcm.3249

Kraft, B., Strous, M., Tegetmeyer, H.E., 2011. Microbial nitrate respiration - Genes, enzymes and environmental distribution. J. Biotechnol. 155, 104–117. https://doi.org/10.1016/j.jbiotec.2010.12.025

Laverman, A.M., Pallud, C., Abell, J., Cappellen, P. Van, 2012. Comparative survey of potential nitrate and sulfate reduction rates in aquatic sediments. Geochim. Cosmochim. Acta 77, 474–488. https://doi.org/10.1016/j.gca.2011.10.033

Mariotti, A., Germon, J.C., Hubert, P., Kaiser, P., Letolle, R., Tardieux, A., Tardieux, P., 1981. Experimental determination of nitrogen kinetic isotope fractionation: Some principles; illustration for the denitrification and nitrification processes. Plant Soil

62, 413–430. https://doi.org/10.1007/BF02374138

Mariotti, A., Landreau, A., Simon, B., 1988. ^{15}N isotope biogeochemistry and natural denitrification process in groundwater: Application to the chalk aquifer of northern France. Geochim. Cosmochim. Acta 52, 1869–1878. https://doi.org/10.1016/0016-7037(88)90010-5

McIlvin, M.R., Altabet, M.A., 2005. Chemical conversion of nitrate and nitrite to nitrous oxide for nitrogen and oxygen isotopic analysis in freshwater and seawater. Anal Chem 77, 5589–5595. https://doi.org/10.1021/ac050528s

Meckenstock, R.U., Morasch, B., Griebler, C., Richnow, H.H., 2004. Stable isotope fractionation analysis as a tool to monitor biodegradation in contaminated acquifers. J. Contam. Hydrol. 75, 215–255. https://doi.org/10.1016/j.jconhyd.2004.06.003

Moreno-vivián, C., Cabello, P., Blasco, R., Castillo, F., Cabello, N., Marti, M., 1999. Prokaryotic Nitrate Reduction : Molecular Properties and Functional Distinction among Bacterial Nitrate Reductases 181, 6573–6584.

Otero, N., Canals, À., Soler, A., 2007. Using dual-isotope data to trace the origin and processes of dissolved sulphate: A case study in Calders stream (Llobregat basin, Spain). Aquat. Geochemistry 13, 109–126. https://doi.org/10.1007/s10498-007-9010-3

Otero, N., Torrentó, C., Soler, A., Menció, A., Mas-Pla, J., 2009. Monitoring groundwater nitrate attenuation in a regional system coupling hydrogeology with multi-isotopic methods: The case of Plana de Vic (Osona, Spain). Agric. Ecosyst. Environ. 133, 103–113. https://doi.org/10.1016/j.agee.2009.05.007

Peng, Y.Z., Ma, Y., Wang, S.Y., 2007. Denitrification potential enhancement by addition of external carbon sources in a pre-denitrification process. J. Environ. Sci.

643 19, 284–289. https://doi.org/10.1016/S1001-0742(07)60046-1

644 Philippot, L., Hallin, S., Schloter, M., 2007. Ecology of Denitrifying Prokaryotes in
645 Agricultural Soil, in: Advances in Agronomy. pp. 249–305.
646 https://doi.org/10.1016/S0065-2113(07)96003-4

647 Richardson, D.J., Watmough, N.J., 1999. Inorganic nitrogen metabolism in bacteria.
648 Curr. Opin. Chem. Biol. 3, 207–219. https://doi.org/10.1016/S1367-
649 5931(99)80034-9

650 Rivett, M.O., Buss, S.R., Morgan, P., Smith, J.W.N., Bemment, C.D., 2008. Nitrate
651 attenuation in groundwater: A review of biogeochemical controlling processes.
652 Water Res. 42, 4215–4232. https://doi.org/10.1016/j.watres.2008.07.020

653 Ryabenko, E., Altabet, M. a., Wallace, D.W.R., 2009. Effect of chloride on the chemical
654 conversion of nitrate to nitrous oxide for $\delta^{15}N$ analysis. Limnol. Oceanogr.
655 Methods 7, 545–552. https://doi.org/10.4319/lom.2009.7.545

656 Schmidt, T.C., Zwank, L., Elsner, M., Berg, M., Meckenstock, R.U., Haderlein, S.B.,
657 2004. Compound-specific stable isotope analysis of organic contaminants in
658 natural environments: A critical review of the state of the art, prospects, and future
659 challenges. Anal. Bioanal. Chem. 378, 283–300. https://doi.org/10.1007/s00216-
660 003-2350-y

661 Sebilo, M., Mayer, B., Nicolardot, B., Pinay, G., Mariotti, A., 2013. Long-term fate of
662 nitrate fertilizer in agricultural soils. Proc. Natl. Acad. Sci. U. S. A. 110, 18185–9.
663 https://doi.org/10.1073/pnas.1305372110

664 Smith, R.L., Miller, D.N., Brooks, M.H., Widdowson, M.A., Killingstad, M.W., 2001. In
665 situ stimulation of groundwater denitrification with formate to remediate nitrate
666 contamination. Environ. Sci. Technol. 35, 196–203.
667 https://doi.org/10.1021/es001360p

668 Strebel, O., Böttcher, J., Fritz, P., 1990. Use of isotope fractionation of sulfate-sulfur
669 and sulfate-oxygen to assess bacterial desulfurication in a sandy aquifer. J.
670 Hydrol. 121, 155–172. https://doi.org/10.1016/0022-1694(90)90230-U

671 Torrentó, C., Urmeneta, J., Otero, N., Soler, A., Viñas, M., Cama, J., 2011. Enhanced
672 denitrification in groundwater and sediments from a nitrate-contaminated aquifer
673 after addition of pyrite. Chem. Geol. 287, 90–101.
674 https://doi.org/10.1016/j.chemgeo.2011.06.002

675 Vidal-Gavilan, G., Folch, A., Otero, N., Solanas, A.M., Soler, A., 2013. Isotope
676 characterization of an in situ biodenitrification pilot-test in a fractured aquifer. Appl.
677 Geochemistry 32, 153–163. https://doi.org/10.1016/j.apgeochem.2012.10.033

678 Vitòria, L., Otero, N., Soler, A., Canals, A., 2004. Fertilizer characterization: Isotopic
679 data (N, S, O, C, and Sr). Environ. Sci. Technol.
680 https://doi.org/10.1021/es0348187

681 Vitòria, L., Soler, A., Aravena, R., Canals, À., 2005. Multi-isotopic approach (^{15}N, ^{13}C,
682 ^{34}S, ^{18}O and D) for tracing agriculture contamination in groundwater, in:
683 Environmental Chemistry: Green Chemistry and Pollutants in Ecosystems.
684 https://doi.org/10.1007/3-540-26531-7_5

685 Vitòria, L., Soler, A., Canals, À., Otero, N., 2008. Environmental isotopes (N, S, C, O,
686 D) to determine natural attenuation processes in nitrate contaminated waters:
687 Example of Osona (NE Spain). Appl. Geochemistry 23, 3597–3611.
688 https://doi.org/10.1016/j.apgeochem.2008.07.018

689 Vitousek, P.M., Aber, J.D., Howarth, R.W., Likens, G.E., Matson, P.A., Schindler, D.W.,
690 Schlesinger, W.H., Tilman, D.G., 1997. Human alteration of the global nitrogen
691 cycle: Sources and consequences. Ecol. Appl. 7, 737–750.
692 https://doi.org/10.1017/CBO9781107415324.004

693 Ward, M.H., DeKok, T.M., Levallois, P., Brender, J., Gulis, G., Nolan, B.T.,
694 VanDerslice, J., 2005. Workgroup Report: Drinking-Water Nitrate and Health—
695 Recent Findings and Research Needs. Environ. Health Perspect. 113, 1607–
696 1614. https://doi.org/10.1289/ehp.8043

697 Wassenaar, L.I., 1995. Evaluation of the origin and fate of nitrate in the Abbotsford
698 Aquifer using the isotopes of ^{15}N and ^{18}O in NO_3^-. Appl. Geochemistry 10, 391–
699 405. https://doi.org/10.1016/0883-2927(95)00013-A

700 Wilderer, P.A., Jones, W.L., Dau, U., 1987. Competition in denitrification systems
701 affecting reduction rate and accumulation of nitrite. Water Res. 21, 239–245.
702 https://doi.org/10.1016/0043-1354(87)90056-X

703 Wunderlich, A., Meckenstock, R., Einsiedl, F., 2012. Effect of different carbon
704 substrates on nitrate stable isotope fractionation during microbial denitrification.
705 Environ. Sci. Technol. 46, 4861–4868. https://doi.org/10.1021/es204075b

706 Wunderlich, A., Meckenstock, R.U., Einsiedl, F., 2013. A mixture of nitrite-oxidizing and
707 denitrifying microorganisms affects the $\delta^{18}O$ of dissolved nitrate during anaerobic
708 microbial denitrification depending on the $\delta^{18}O$ of ambient water. Geochim.
709 Cosmochim. Acta 119, 31–45. https://doi.org/10.1016/j.gca.2013.05.028

710 Zumft, W.G., 1997. Cell biology and molecular basis of denitrification. Microbiol. Mol.
711 Biol. Rev. 61, 533–616.

712

713 **FIGURE CAPTIONS**

714 **Figure 1. Pilot-plant scheme.** Location, schematic map and cross-section of the pilot-
715 plant. I1 and I2 are the injection wells; PZ1, PZ2 and PZ3 the monitoring piezometers;
716 EW the extraction well and MW the monitoring well. I2 is projected on the cross-section.

717 Arrows depict the flow direction when the EW is operating. Natural flow direction is from
718 I1 to MW.

719 **Figure 2**. **NO_3^- and NO_2^- evolution in the microcosms.** NO_3^- (**A**) and NO_2^- (**B**)
720 concentration in the biostimulated and control microcosms. C1 (black cross):
721 groundwater + sediment, C2 (black triangles): MilliQ water + sediment, C3 (grey
722 squares): groundwater + CH_3COOH, B (grey circles): groundwater + sediment +
723 CH_3COOH.

724 **Figure 3. NO_3^- isotopic fractionation in the microcosms.** Samples from the
725 biostimulated microcosms (black) and initial MW groundwater (empty) isotopic
726 composition.

727 **Figure 4. $\delta^{15}N$ vs $\delta^{18}O$ diagram from field samples.** Isotopic results from the
728 piezometers and the EW (circles) samples and mean value of the unaffected MW
729 (square), including standard deviation. The regression line is presented as a continuous
730 black line (slope = 0.7 (r^2 = 0.95)). The boxes (grey continuous and dashed lines)
731 represent NO_3^- sources from Vitòria et al., 2004 and references therein.

732 **Figure 5**. **NO_3^- evolution in the pilot-plant.** The dashed grey line corresponds to the
733 MW mean concentration. Empty symbols for PZ1 and PZ2 correspond to bottom
734 samples (two-depth sampling). The vertical line corresponds to the last injection date.

735 **Figure 6**. **Pilot-plant SO_4^{2-} concentration and isotopic composition.** The regression
736 line is presented as a dashed black line (slope = 0.4 (r^2 = 0.93)). The boxes, including
737 standard deviation, represent SO_4^{2-} sources from Otero et al., (2007); Vitòria et al.,
738 (2004) and references therein.

739 **Figure 7. Representative sampling campaigns from the pilot-plant. A)** 1st month (1.2
740 slope (r^2 = 0.45)); **B)** 7th month, 0.5 slope (r^2 = 0.8); **C)** 12th month, 0.6 slope (r^2 = 0.9); **D)**
741 19th month, 0.8 slope (r^2 = 1.0); **E)** 24th month, 0.6 slope (r^2 = 1.0). Regression line for

each campaign is presented as a dashed line. The DEN % line (continuous line) was calculated using the isotopic fractionation values obtained in the laboratory experiments, and the average concentration and isotopic composition of the MW as initial values.

Figure S1. NO_2^- evolution during the pilot plant operation. NO_2^- concentration of the pilot plant samples. Empty symbols for PZ1 and PZ2 correspond to bottom samples (two-depth sampling). The vertical line corresponds to the last injection date.

Figure S2. Temporal dynamics of the NO_3^- isotopic composition. A) $\delta^{15}N\text{-}NO_3^-$ and **B**) $\delta^{18}O\text{-}NO_3^-$ measured in the samples collected in the pilot-plant. The dashed grey line corresponds to the MW average composition. The vertical line corresponds to the last injection date. Empty symbols for PZ2 correspond to bottom samples (two-depth sampling).

Figure S3. Rainfall data. Rainfall (mm) registered each sampling campaign day (striped bar) and the previous six days (dark to light grey colour). The data was recorded by station 0252D from the Spanish national meteorological agency (AEMET, Ministry of Agriculture, Food and Environment of Spain),

Table 1. Batch experiments set-up. Composition for each microcosm.

Table 2. Groundwater mixing at EW. Theoretical mixing calculation between 30 % of PZ2 and 70 % of MW using chemical and isotopic data (E), compared with the measured (M) NO_3^- concentration and isotopic composition at the EW. Standard deviation (SD) is included.

Table S1. Batch experiments results. Chemical and isotopic characterization of the samples obtained from the sacrificed microcosms. “n.d.” refers to parameters that were not determined.

Table S2. Pilot-plant results. Chemical and isotopic characterization of the samples obtained from the pilot-plant. “n.d.” refers to parameters that were not determined.

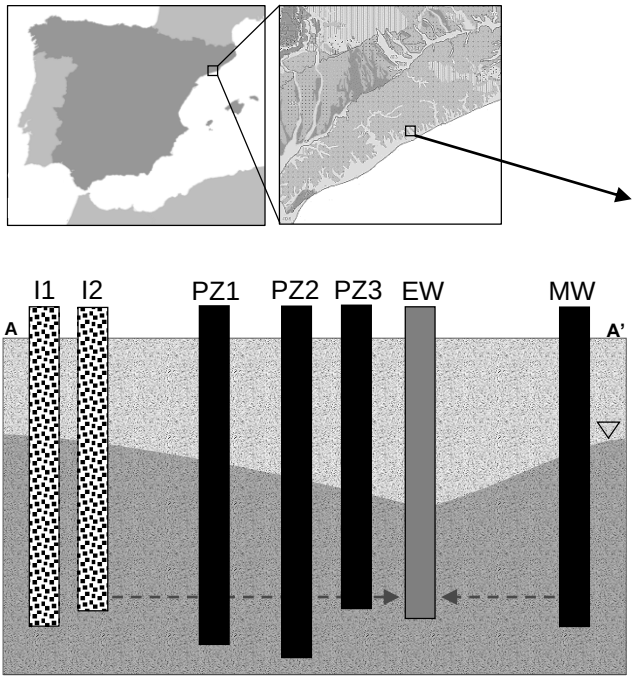
I1
I2
PZ1
PZ2
PZ3
EW
MW
A
A'
Stream
Water flow
10 m

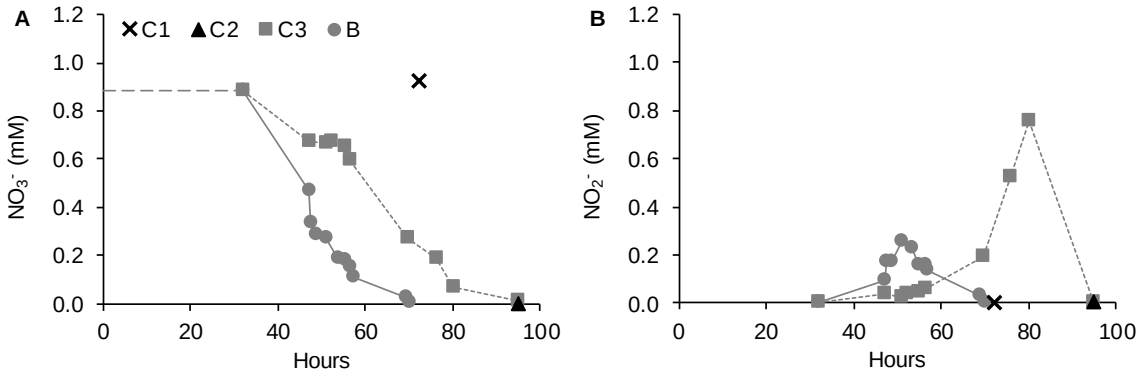
A
C1
C2
C3
B
1.2
1.0
0.8
0.6
0.4
0.2
0.0
NO_3^- (mM)
0
20
40
60
80
100
Hours
B
1.2
1.0
0.8
0.6
0.4
0.2
0.0
NO_2^- (mM)
0
20
40
60
80
100
Hours

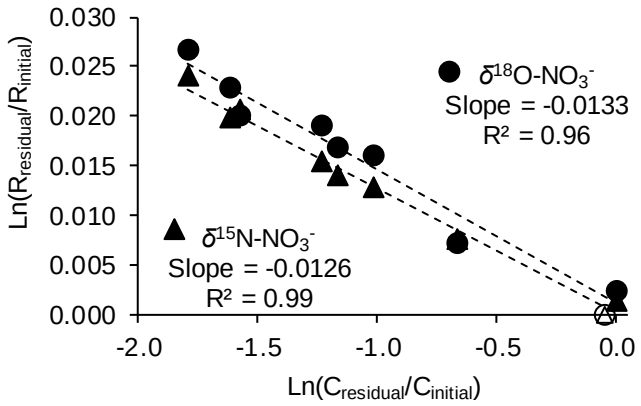
0.030
0.025
0.020
0.015
0.010
0.005
0.000
-2.0
-1.5
-1.0
-0.5
0.0
Ln(Rresidual/Rinitial)
Ln(Cresidual/Cinitial)
δ18O-NO3-
Slope = -0.0133
R² = 0.96
δ15N-NO3-
Slope = -0.0126
R² = 0.99

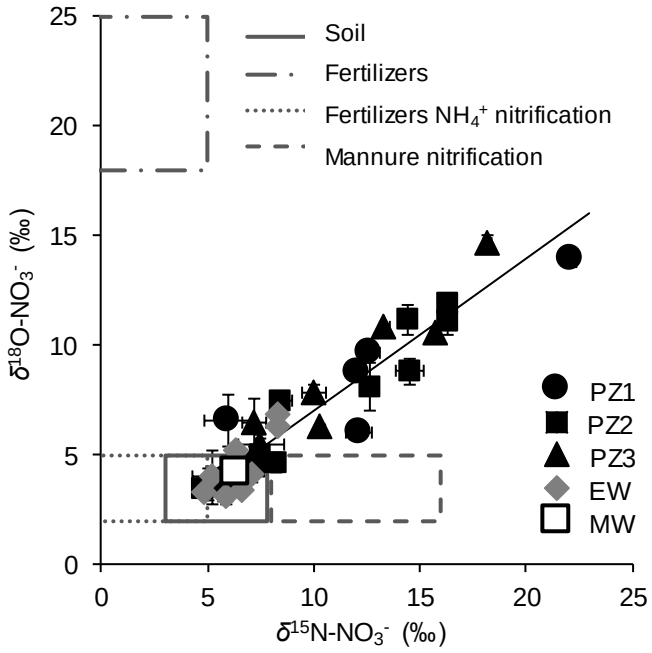
Soil
Fertilizers
Fertilizers NH4+ nitrification
Mannure nitrification
PZ1
PZ2
PZ3
EW
MW
δ18O-NO3- (‰)
δ15N-NO3- (‰)
0
5
10
15
20
25

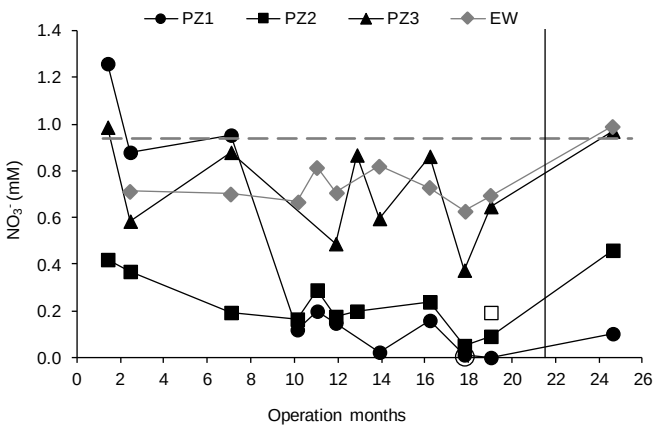
PZ1
PZ2
PZ3
EW
1.4
1.2
1.0
0.8
0.6
0.4
0.2
0.0
NO_3^- (mM)
0
2
4
6
8
10
12
14
16
18
20
22
24
26
Operation months

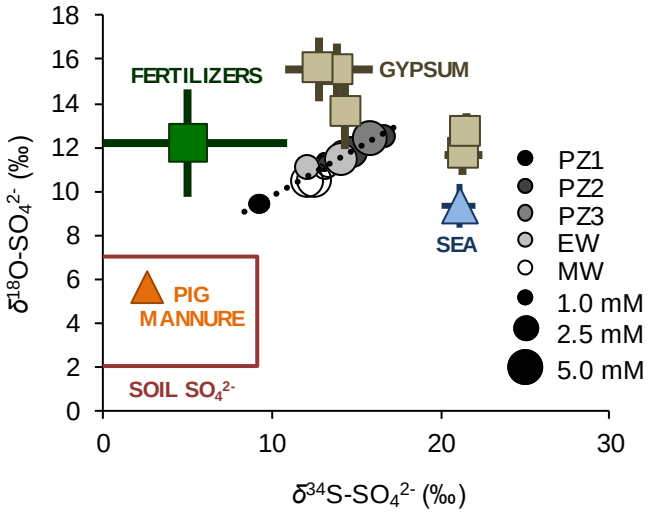
FERTILIZERS
GYPSUM
SEA
PIG MANNURE
SOIL SO_4^{2-}
PZ1
PZ2
PZ3
EW
MW
1.0 mM
2.5 mM
5.0 mM
$\delta^{18}O\text{-}SO_4^{2-}$ (‰)
$\delta^{34}S\text{-}SO_4^{2-}$ (‰)
0
2
4
6
8
10
12
14
16
18
0
10
20
30

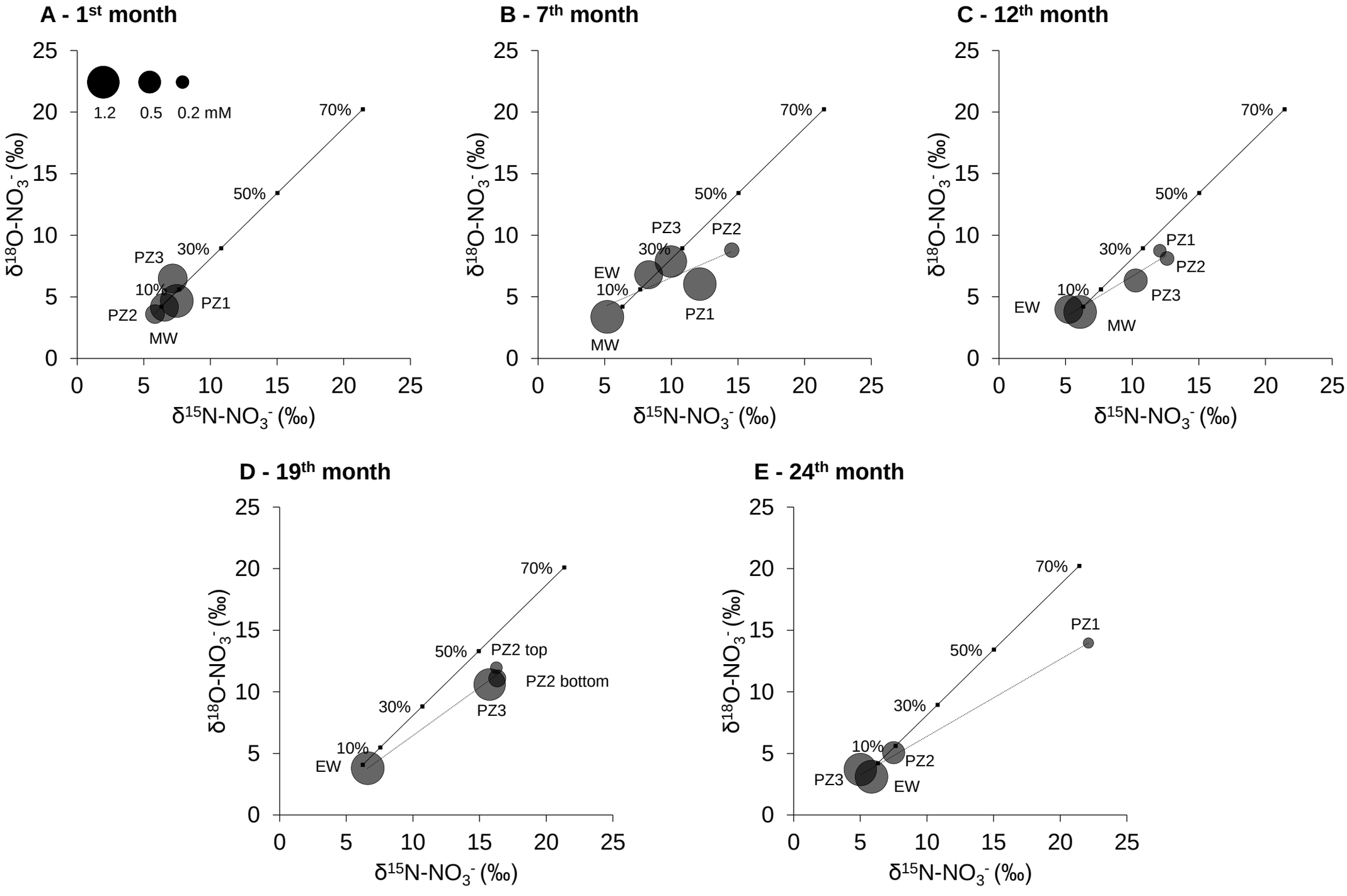
A - 1st month
B - 7th month
C - 12th month
D - 19th month
E - 24th month
1.2
0.5
0.2 mM
70%
50%
30%
10%
PZ1
PZ2
PZ3
EW
MW
PZ2 top
PZ2 bottom
δ18O-NO3- (‰)
δ15N-NO3- (‰)
0
5
10
15
20
25

Reactor	Code	Water source	Water volume (mL)	Flask volume (mL)	Sediment (g)	CH_3COOH 85% (µL)
Stimulated	B1-B10	MW	150	250	20	33
Control 1	C1	MW	150	250	20	0
Control 2	C2	Milli-Q	150	250	20	0
Control 3	C3	MW	300	500	0	66

	NO_3^- (mM)			$\delta^{15}N\text{-}NO_3^-$ (‰)			$\delta^{18}O\text{-}NO_3^-$ (‰)		
Month	**E**	**M**	**SD**	**E**	**M**	**SD**	**E**	**M**	**SD**
1	0.78	-	-	6.2	-	-	4.0	-	--
2	0.77	0.71	0.04	5.8	8.3	1.7	4.0	6.7	1.6
7	0.72	0.70	0.01	8.8	8.3	0.3	5.6	6.8	0.9
10	0.71	0.67	0.03	6.9	4.9	1.4	4.3	3.3	0.8
11	0.74	0.82	0.05	7.0	6.3	0.5	5.2	5.2	0.0
12	0.71	0.71	0.00	8.2	5.2	2.1	5.4	4.0	1.0
14	0.66	0.82	0.12	4.4	6.6	1.6	3.0	3.4	0.3
17	0.67	0.63	0.03	8.8	7.1	1.2	6.3	4.1	1.6
19	0.69	0.69	0.01	9.3	6.6	2.0	6.5	3.8	1.9
24	0.80	0.99	0.14	6.7	5.8	0.6	4.5	3.1	1.0

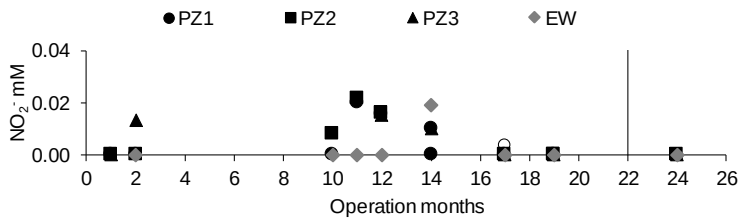
PZ1
PZ2
PZ3
EW
0.04
0.02
0.00
NO_2^- mM
0
2
4
6
8
10
12
14
16
18
20
22
24
26
Operation months

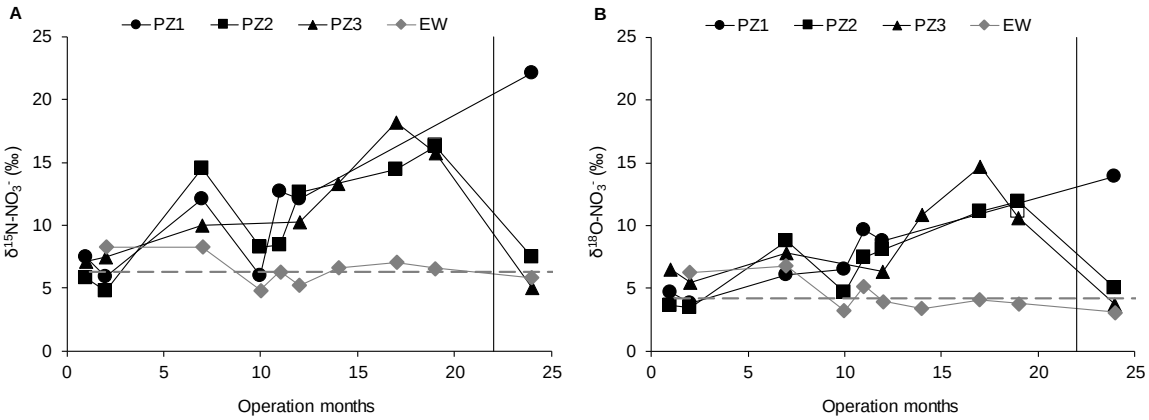
A
PZ1
PZ2
PZ3
EW
δ15N-NO3- (‰)
Operation months
B
PZ1
PZ2
PZ3
EW
δ18O-NO3- (‰)
Operation months

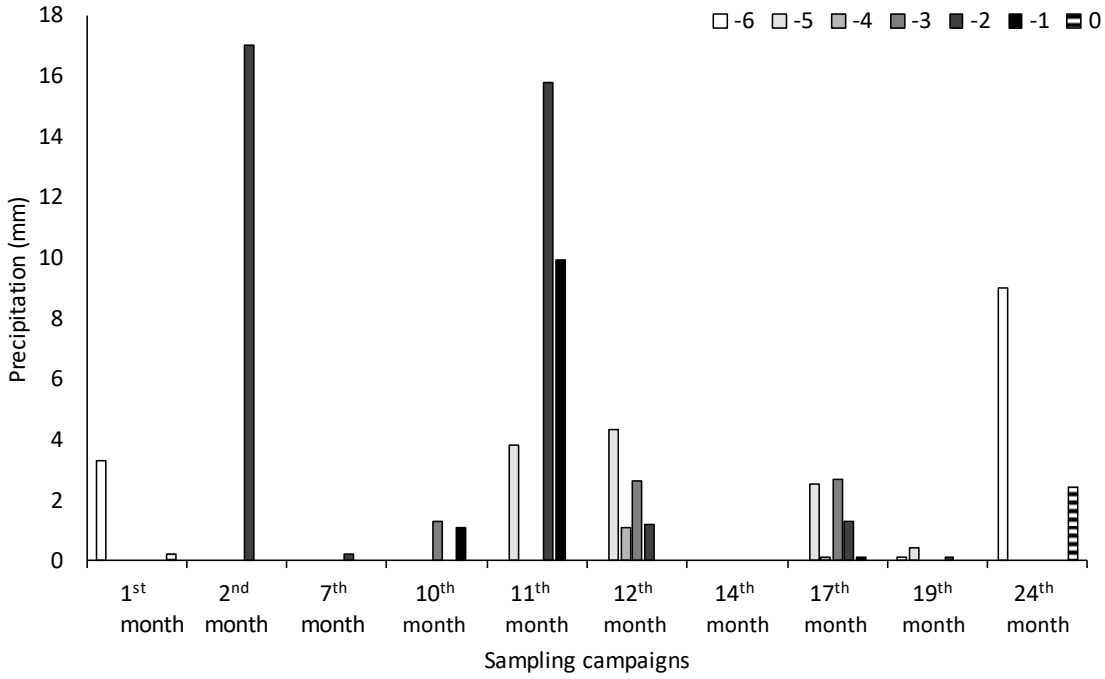
-6 -5 -4 -3 -2 -1 0
Precipitation (mm)
18
16
14
12
10
8
6
4
2
0
1st month
2nd month
7th month
10th month
11th month
12th month
14th month
17th month
19th month
24th month
Sampling campaigns

CODE	HOUR	NO_3^- (mM)	NO_2^- (mM)	$\delta^{15}N\text{-}NO_3^-$ (‰)	$\delta^{18}O\text{-}NO_3^-$ (‰)	SD $\delta^{15}N\text{-}NO_3^-$	SD $\delta^{18}O\text{-}NO_3^-$	NH_4^+ (mM)
GW	0.0	0.89	0.01	5.0	3.6	0.3	1.4	n.d.
B-1	47.0	0.47	0.09	12.6	10.8	0.3	0.1	0.00
B-2	47.5	0.33	0.17	17.9	19.9	1.1	0.9	0.00
B-3	48.5	0.29	0.17	19.2	20.7	1.1	0.3	0.03
B-4	51.0	0.27	0.26	20.7	23.0	1.7	0.5	0.03
B-5	53.5	0.19	0.23	26.0	24.0	n.d.	n.d.	0.03
B-6	55.0	0.18	0.16	25.1	26.7	0.3	1.4	0.01
B-7	56.5	0.15	0.16	29.7	30.7	0.3	1.9	0.02
B-8	57.0	0.11	0.14	n.d.	n.d.	n.d.	n.d.	0.01
B-9	69.0	0.03	0.03	n.d.	n.d.	n.d.	n.d.	0.02
B-10	70.0	0.01	0.00	n.d.	n.d.	n.d.	n.d.	0.02
C1	72.0	0.92	0.00	6.5	6.0	0.9	0.3	0.04
C2	72.0	0.00	0.00	n.d.	n.d.	n.d.	n.d.	n.d.
C3-1	32.0	0.89	0.00	n.d.	n.d.	n.d.	n.d.	n.d.
C3-2	47.0	0.67	0.04	n.d.	n.d.	n.d.	n.d.	n.d.
C3-3	51.0	0.67	0.03	n.d.	n.d.	n.d.	n.d.	n.d.
C3-4	52.3	0.67	0.04	n.d.	n.d.	n.d.	n.d.	n.d.
C3-5	55.0	0.65	0.05	n.d.	n.d.	n.d.	n.d.	n.d.
C3-6	56.5	0.60	0.06	n.d.	n.d.	n.d.	n.d.	n.d.
C3-7	69.5	0.27	0.19	n.d.	n.d.	n.d.	n.d.	n.d.
C3-8	76.0	0.19	0.53	n.d.	n.d.	n.d.	n.d.	n.d.
C3-9	80.0	0.07	0.76	n.d.	n.d.	n.d.	n.d.	n.d.
C3-10	95.0	0.01	0.00	n.d.	n.d.	n.d.	n.d.	n.d.

Code	Month	NO_3^- (mM)	NO_2^- (mM)	$\delta^{15}N\text{-}NO_3^-$ (‰)	$\delta^{18}O\text{-}NO_3^-$ (‰)	SD $\delta^{15}N\text{-}NO_3^-$	SD $\delta^{18}O\text{-}NO_3^-$	SO_4^{2-} (mM)	$\delta^{34}S\text{-}SO_4^{2-}$ (‰)	$\delta^{18}O\text{-}SO_4^{2-}$ (‰)	SD $\delta^{18}O\text{-}SO_4^{2-}$	Denitrif. % (concentration)	Denitrif. % (isotopes)
PZ1	1	1.26	0.00	7.5	4.7	0.6	0.0	1.72	9.2	9.4	0.3	0	7
PZ2		0.42	0.00	5.8	3.6	0.6	0.8	1.04	13.1	11.3	0.1	55	0
PZ3		0.98	0.00	7.2	6.5	0.5	1.1	2.79	n.d.	n.d.	n.d.	0	5
W2		0.92	0.00	6.5	4.2	0.6	1.5	2.43	13.3	11.2	0.1	0	0
PZ1	2	0.88	0.00	5.9	3.8	0.1	0.5	1.40	n.d.	n.d.	n.d.	6	0
PZ2		0.37	0.00	4.7	3.5	0.5	0.1	1.13	13.1	11.4	0.1	61	0
PZ3		0.58	0.01	7.5	5.5	1.1	0.5	2.56	n.d.	n.d.	n.d.	38	0
W1		0.71	0.00	8.3	6.3	0.3	0.2	2.04	14.1	11.8	0.3	24	0
W2		0.97	0.00	8.7	5.7	0.3	0.1	2.34	13.1	11.1	0.2	0	0
PZ1	7	0.95	n.d.	12.1	6.0	0.6	0.0	0.00	n.d.	n.d.	n.d.	0	42
PZ2		0.19	n.d.	14.5	8.8	0.6	0.6	0.00	n.d.	n.d.	n.d.	79	52
PZ3		0.88	n.d.	10.0	7.9	0.6	0.3	0.00	n.d.	n.d.	n.d.	6	31
W1		0.70	n.d.	8.3	6.8	0.1	0.3	0.00	n.d.	n.d.	n.d.	25	22
W2		0.96	n.d.	5.2	3.4	0.5	1.2	0.00	n.d.	n.d.	n.d.	0	0
PZ1	10	0.12	0.00	6.0	6.5	1.1	1.2	1.58	n.d.	n.d.	n.d.	87	7
PZ2		0.16	0.01	8.2	4.7	0.2	0.5	1.90	n.d.	n.d.	n.d.	82	22
W1		0.67	0.00	4.9	3.2	0.3	0.1	2.41	n.d.	n.d.	n.d.	29	0
W2		0.88	0.00	5.0	3.6	0.3	1.4	2.45	n.d.	n.d.	n.d.	0	0
PZ1	11	0.20	0.02	12.7	9.7	0.4	0.1	2.80	14.1	11.4	n.d.	79	40
PZ2		0.29	0.02	8.5	7.5	0.5	0.2	4.07	14.7	11.8	n.d.	69	16
W1		0.82	0.00	6.3	5.2	0.3	0.1	4.24	14.1	11.5	0.1	13	0

W2		0.93	0.00	6.3	4.6	0.1	0.2	4.12	12.0	10.5	0.1	0	0
PZ1		0.15	0.02	12.1	8.7	0.3	0.2	0.66	n.d.	n.d.	n.d.	84	38
PZ2		0.18	0.02	12.6	8.1	0.2	1.1	2.46	16.6	12.5	0.2	81	40
PZ3	12	0.49	0.02	10.3	6.3	0.0	0.1	5.07	15.8	12.4	0.0	48	28
W1		0.71	0.00	5.2	4.0	1.0	1.3	2.82	12.1	11.1	0.2	25	0
W2		0.97	0.00	6.1	3.8	0.2	0.9	4.89	12.5	10.5	0.0	0	0
PZ1		0.02	0.01	n.d.	n.d.	n.d.	n.d.	2.42	n.d.	n.d.	n.d.	98	100
PZ3	14	0.59	0.01	13.3	10.8	0.2	0.1	3.37	n.d.	n.d.	n.d.	37	41
W1		0.82	0.02	6.6	3.4	0.2	0.2	2.61	n.d.	n.d.	n.d.	13	0
PZ145		0.00	0.00	n.d.	n.d.	n.d.	n.d.	1.12	n.d.	n.d.	n.d.	100	100
PZ139		0.01	0.00	n.d.	n.d.	n.d.	n.d.	1.15	n.d.	n.d.	n.d.	99	100
PZ237	17	0.05	0.00	14.4	11.2	0.2	0.7	1.66	n.d.	n.d.	n.d.	95	44
PZ3		0.37	0.00	18.2	14.7	0.1	0.4	2.28	n.d.	n.d.	n.d.	60	58
W1		0.63	0.00	7.1	4.1	0.2	0.4	2.11	n.d.	n.d.	n.d.	33	0
PZ1		0.00	0.01	n.d.	n.d.	n.d.	n.d.	n.d.	n.d.	n.d.	n.d.	100	100
PZ245		0.19	0.02	16.3	11.1	0.1	0.6	n.d.	n.d.	n.d.	n.d.	79	54
PZ238	19	0.09	0.01	16.3	12.0	0.1	0.1	n.d.	n.d.	n.d.	n.d.	90	53
PZ3		0.64	0.06	15.8	10.6	0.1	0.1	n.d.	n.d.	n.d.	n.d.	31	51
W1		0.69	0.00	6.6	3.8	0.3	0.5	n.d.	n.d.	n.d.	n.d.	26	0
PZ1	24	0.10	0.01	22.1	14.0	0.1	0.3	n.d.	n.d.	n.d.	n.d.	89	72

PZ2 45	0.46	0.02	7.5	5.1	0.0	0.7	n.d.	n.d.	n.d.	n.d.	51	12
PZ3	0.97	0.00	5.0	3.7	0.2	0.7	n.d.	n.d.	n.d.	n.d.	0	0
W1	0.99	0.00	5.8	3.1	0.3	0.0	n.d.	n.d.	n.d.	n.d.	0	0